Chapter 15
All-Cellulosic Based Composites

J.P. Borges, M.H. Godinho, J.L. Figueirinhas, M.N. de Pinho, and M.N. Belgacem

Abstract The use of cellulosic fibers as load bearing constituents in composite materials has increased over the last decade due to their relative cheapness compared to conventional materials such as glass and aramid fibers, their ability to recycle, and because they compete well in terms of strength per weight of material. All-cellulosic based composites prepared from cellulose derivatives based matrices and microcrystalline cellulosic fibers made by direct coupling between fibers and matrix present interesting mechanical and gas permeation properties, thus being potential candidates for packaging materials. Both the cellulosic matrix and the reinforcing fibers are biocompatible and widely used in the pharmaceutical industry, which is very important for the envisaged application. In addition to their biocompatibility, cellulosic systems have the ability to form both thermotropic and lyotropic chiral nematic phases, and the composites produced from the latter show improved mechanical properties due to fiber orientation induced by the anisotropic matrix. The preparation and characterization (morphological, topographical, mechanical, gas barrier properties) of all-cellulosic based composites are described in this chapter.

Keywords Cellulose fibers · Composites · Hydroxypropylcellulose · Liquid crystals

Contents

J.P. Borges (✉)
Departamento de Ciência dos Materiais and CENIMAT/I3N, FCT, Universidade Nova de Lisboa, 2829-516 Caparica, Portugal
e-mail: jpb@fct.unl.pt

S. Kalia et al. (eds.), *Cellulose Fibers: Bio- and Nano-Polymer Composites*,
DOI 10.1007/978-3-642-17370-7_15, © Springer-Verlag Berlin Heidelberg 2011

15.1 Introduction

The important feature of composite materials is that they can be designed and tailored to meet different requirements, since the overall mechanical properties of a starting material (the matrix) can be improved by the addition of a reinforcing agent [1]. Owing to increasing environmental concerns, the use and removal of traditional polymeric composite structures, usually made of epoxy, unsaturated polyester or phenolic resins reinforced with glass, carbon, or aramid fibers has been criticized. Recently, composite materials based on cellulose and/or its derivatives have been the subject of intense research [2–12]. The reason for this resides in the renewable and biodegradable character of cellulose, and also in the fact that (a) it is abundant and inexpensive; (b) nature provides a large variety of cellulosic fibers in terms of morphology, geometry, and surface properties, depending on the source and/or separation process; and (c) in terms of specific strength, cellulosic fibers can be compared with the extensively used glass fibers. Moreover, cellulose-based composites are easy to recycle at the end of their life cycle, either by reprocessing (thermoplastic matrices) or by energy recovery (combustion of thermoset composites), which does not leave any residue since they are based on two organic components.

The major drawback of cellulose fibers in the present context resides in their highly polar and hydrophilic character, which make them both poorly compatible with commonly used non-polar matrices, such as polyolefins, and subject to loss of mechanical properties upon atmospheric moisture absorption. That is why they should be submitted to specific surface modifications in order to obtain an efficient hydrophobic barrier and to minimize their interfacial energy with the often non-polar polymer matrix, and thus generate optimum adhesion. Further improvement of this interfacial strength, which is a basic requirement for the optimized mechanical performance of any composite, is attained by chain entanglement between the matrix macromolecules and the long chains appended to the fiber surface (brushes) or, better still, by the establishment of a continuity of covalent bonds at the interface between the two components of the composite.

Several fiber treatments are reported in literature [9], namely (a) physical treatments, such as solvent extraction; (b) physico-chemical treatments, like the use of corona and plasma discharges or laser, γ-ray and UV bombardment and (c) chemical modifications, both by the direct condensation of the coupling agents onto the cellulose surface and by various grafting strategies calling upon polycondensations and free-radical or ionic polymerizations.

Another approach to enhance interfacial bonding was proposed by Borges et al. [10], and deals with the direct coupling between the matrix and the reinforcing fibers. The elaboration of the composite is based on using a cellulose derivative based matrix and diisocyanates as coupling agents. To the best of our knowledge, this was the first attempt to the production of all-cellulosic based composites. These soft materials (sub-ambient glass transition temperature) are insoluble, meaning that the isocyanates also promote a cross-linking reaction between the anhydroglucose units of the matrix (see Fig. 15.1) [13]. These properties along with mechanical and

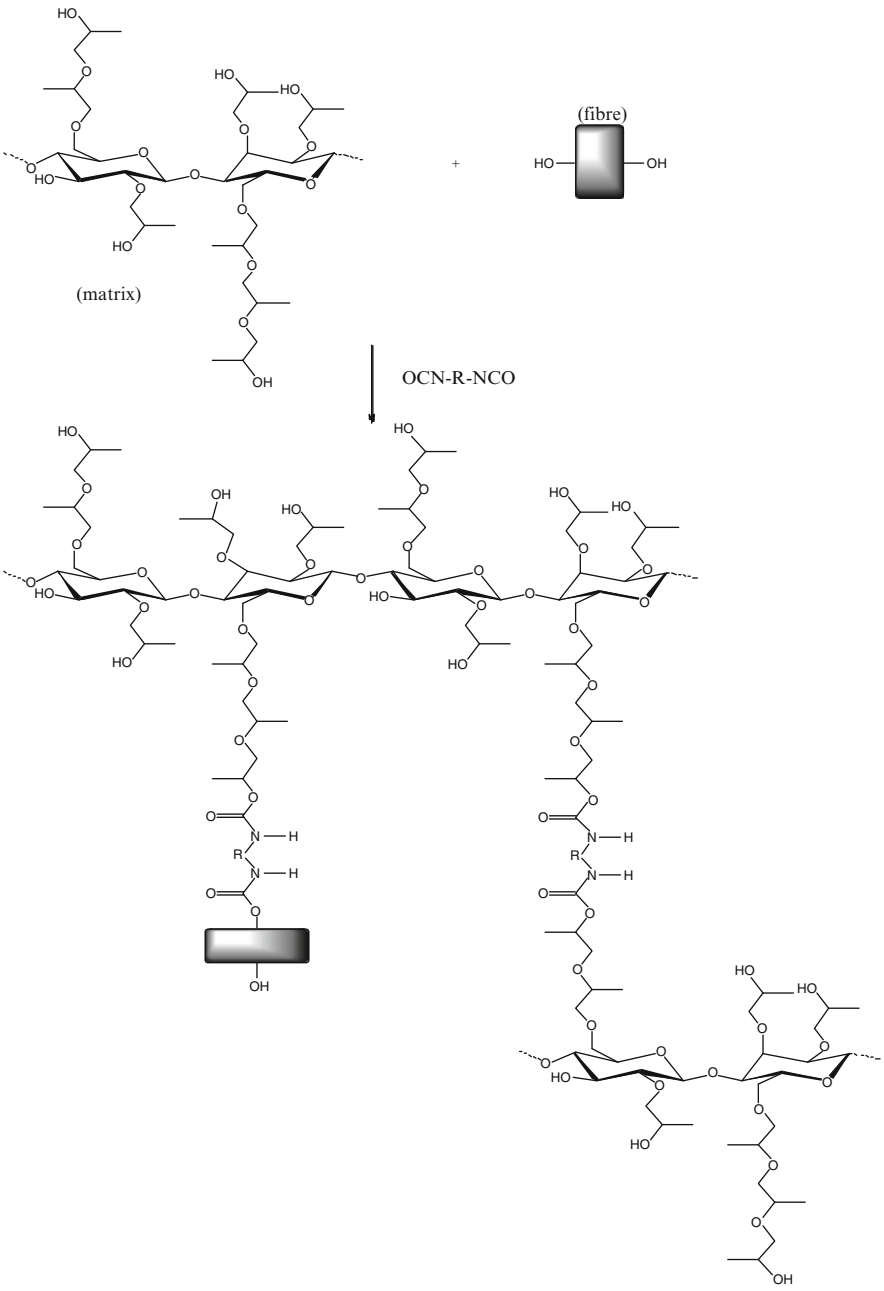

Fig. 15.1 Schematics of competitive chemical bonds promoted by diisocyanates in all-cellulosic based composites. Chemical coupling between fibers and matrix and cross-linking between anhydroglucose units of the matrix are shown. R refers to an aliphatic or aromatic group. The matrix is hydroxypropylcellulose (HPC)

gas barrier properties, which are analyzed in this chapter, make these materials suitable for packaging applications.

The designation "all-cellulosic based composites" is used throughout this chapter that focuses on the production and characterization of these materials.

15.2 All-Cellulosic Based Composites Preparation Methodology

An ester of cellulose, the hydroxypropylcellulose (HPC), was chosen among the several cellulosic derivatives which can be used as matrix materials. HPC is readily available, inexpensive and soluble in a wide variety of common organic solvents. As reinforcement, Avicel fibers ($l = 30$ μm and $l/d = 5$) were used. Cross-linking was achieved using several aliphatic or aromatic diisocyanates [13]. It is worth mention that general trends concerning the mechanical and gas barrier properties were similar for all cross-linked composites, and for that reason we refer to those that have been cross-linked with 1,4-butyldiisocyanate (BDI).

The all-cellulosic based composites were prepared in the form of dense films (thickness: 20–60 μm). Clear composite films were obtained either from isotropic or liquid crystalline solutions of HPC (chiral nematic) by a casting method.

Isotropic solutions of HPC (10–12% wt HPC) were prepared by mixing acetone with HPC at room temperature. Avicel fibers were added (0, 2, 4, 10, 15, 20 and 30% w/w HPC) to these solutions and the mixture was left to homogenize, by magnetic stirring, for 24 h. Two sets of isotropic composite films were obtained from these solutions. In the first set, the films were cast and sheared over a teflon substrate with a knife edge moving at a calibrated speed. In the second set, the cross-linked films were obtained by first promoting the reaction of BDI (7% w/w HPC) under nitrogen atmosphere with HPC-Avicel. After the cross-linking the films were obtained as described above.

Anisotropic solutions of HPC (60% wt HPC) were prepared by mixing *N*,*N*-dimetylacetamide (DMAc) with HPC at room temperature. Avicel fibers were added (0, 2, 4, 6, 10 and 12% w/w HPC) to these solutions and the mixture was left to homogenize, by mechanical stirring, for 24 h. Anisotropic composite films were obtained by the above mentioned method. In this case cross-linked films were not produced.

15.3 Microstructural Properties

Microstructural evaluation of the composite films was accomplished using two different microscopy techniques: POM and AFM. These two techniques gave information at different levels about the texture (morphology), uniformity and topography of the composites. Birefringence measurements and SALS gave complementary information about the degree of molecular orientation in the matrix and fiber orientation in the composites, respectively.

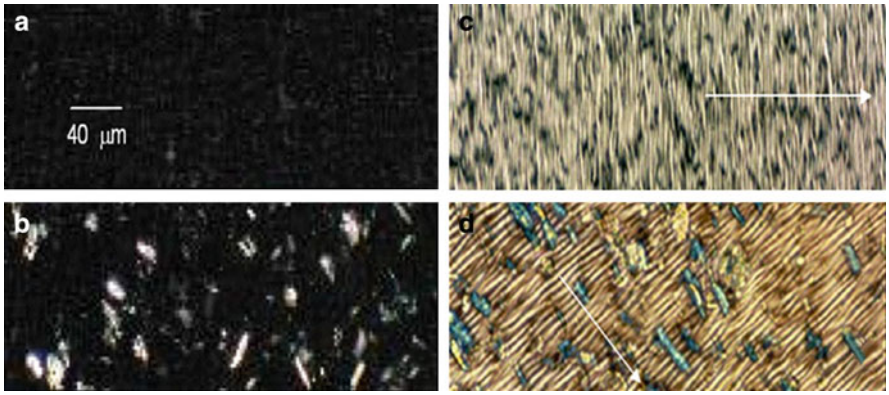

Fig. 15.2 POM photographs of isotropic (**b**) and anisotropic (**d**) all-cellulosic based composites with 4% w/w HPC of Avicel fibers [birefringent rods in images (**b**) and (**d**), respectively]. Images (**a**) and (**c**) are the POM photographs of the isotropic (**a**) and anisotropic (**c**) HPC matrix. *White arrows* in images (**c**) and (**d**) indicate the shear direction. All images were taken under crossed polars. Images were obtained from references [12] (**a** and **b**) and [14] (**c** and **d**)

POM images (taken on an Olympus BH2 microscope) of isotropic and anisotropic all-cellulosic based composites are shown in Fig. 15.2.

POM shows that solid films cast from 10 to 12% wt HPC are isotropic (Fig. 15.2a) (dark field under crossed polars). In contrast, solid films cast from a chiral nematic solution of HPC (60% HPC/40% DMAc, w/w) are clearly birefringent (anisotropic) and present a characteristic banded texture perpendicular to the shear direction, observed for thermotropic and lyotropic liquid crystalline phases of HPC after shear.

The formation of banded textures in thin-film samples of solutions of liquid crystalline polymers (LCPs), subjected to shear, has been reported in the literature since 1979 [15]. Because of the symmetrical properties of the liquid crystal solutions, large domains of well-oriented polymer chains are formed during shear flow, while defects are squeezed into small regions. The shear accounts for an additional energy stored in the solution. When the shear is stopped, the system will first relax with a characteristic time t_b to a transient state. In this state the distortion energy is minimized, and the orientational order is kept, resulting in a banded structure.

This behavior is observed only if two conditions are fulfilled [16]:

1. If the shear rate, $\dot{\gamma}$, is higher than a critical shear rate, $\dot{\gamma}^c$, with $\dot{\gamma}^c$ being strongly dependent on the molecular weight, M, of the polymer and slightly sensitive to the polymer concentration, C, according to the relation $\dot{\gamma}^c \propto C^{-1}M^{-7}\log M$.
2. If the shearing time, t_s, is longer than a critical time, that depends on the shear rate. This means that there is a minimum deformation, γ^c, below which the periodic structure was not observed. The general dependency of the band formation time, t_b, on the experimental parameters is known [16] (e.g., in the first approximation $t_b \sim t_s^{-2}$, t_b increases with the molecular weight M), but no analytical expression was yet deduced, due to the complexity of the dynamic behavior of LCPs under shear.

Band structure may be characterized by the band spacing (typically 4–10 μm) [17] and is energetically very stable, but it only persists during a characteristic time t_d (typically t_d ~10 min). The thermal agitation may be sufficient for the system to overcome the energy barrier between the band texture (local minimum) and the nondistorted state (overall minimum). The bands begin to lose their parallel orientation; they form elongated domains and finally collapse, giving rise to an equilibrium texture near the undeformed state. As expected, the time t_d is found to be strongly dependent [16] on the molecular weight (t_d increases with increasing M) and on the shear rate (t_d increases with increasing $\dot{\gamma}$).

The HPC lyotropic solutions are, regarding the ability to form band texture, among the most studied systems and thoroughly described in the literature [16, 18]. The formed periodic structures can be locked within the polymer after the solvent evaporation, if the evaporation time is shorter than the relaxation time t_d, and the topography can be tuned by control of the processing conditions [19]. In the case of the anisotropic all-cellulosic based composites this was attained due to the small thickness of the films (20–60 μm).

Another interesting feature of these anisotropic composites is their ability to orient the fibers (see Fig. 15.2d) in contrast to isotropic homologues, where no overall orientation of the fibers is achieved (see Fig. 15.2b), which means that this orientation is due to a competition between the alignment promoted by the matrix and the shear.

Fiber alignment in short fiber composites (SFCs) is very difficult to achieve, however the results obtained with anisotropic all-cellulosic based composites point out for a simple and new way of producing fiber aligned SFCs with enhanced mechanical properties, as discussed later on.

Small angle light scattering and birefringence experiments showed a direct correlation between the director alignment in the anisotropic matrix and the orientation of the cellulosic fibers in these composites.

From SALS patterns an order parameter, $S = \frac{1}{2}\left\langle 3\cos^2\theta - 1\right\rangle$, was determined. This parameter gives the degree of orientation of the fibers in the composites. It is expressed as the average ($\langle\rangle$) of the second Legendre polynomial of the cosine function of the angle in between the fibers axes and the shear direction (θ). The order parameter is 0 for a random orientation of the fibers and 1 for its total alignment with the shear direction.

Figure 15.3 presents the variation of the order parameter as a function of HPC concentration in the precursor solutions for the composites made with 2% w/w HPC of Avicel fibers. Similar trends are observed for other fiber contents.

As expected, results in Fig. 15.3 show that significant fiber orientation is only achieved when the matrix is anisotropic. Similar conclusions can be drawn from birefringence measurements (made by the compensation method, using a Berek compensator) on composite films, as shown in Fig. 15.4. The birefringence is a measure of the degree of order of the matrix and therefore the good agreement between these data and those obtained from SALS (S) reveal the excellent compatibility between the matrix and the fibers, which results from a similarity between the chemical structure of both components of the composites.

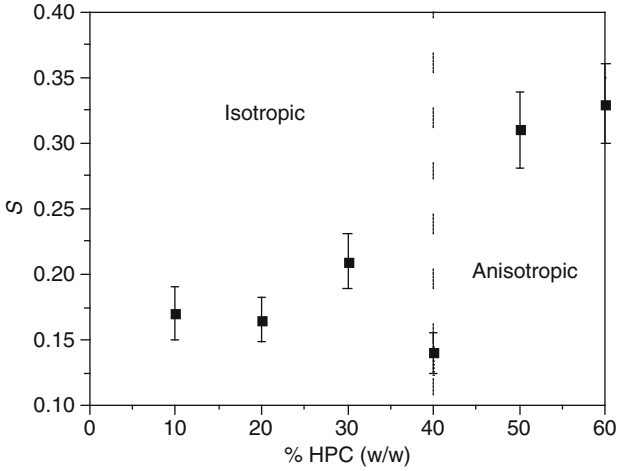

Fig. 15.3 Plot of the order parameter, *S*, for all-cellulosic based composites (2% w/w HPC of Avicel fibers), as a function of the HPC content. Isotropic and anisotropic composites are marked [13]

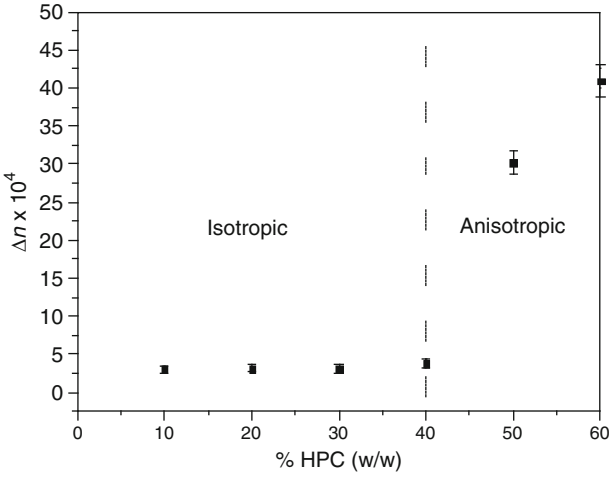

Fig. 15.4 Variation of the birefringence, Δn, of all-cellulosic based composites (2% w/w HPC of Avicel fibers) with the HPC content. Isotropic and anisotropic composites are marked [13]

The surface topography of the films was analyzed using an atomic force microscope from Digital Instruments, Multimode Scanning Probe Microscope with a Nanoscope IIIa Controller. The film surface was scanned in intermediate contact (tapping mode) with an oscillating tip. This eliminates shear forces, which can damage soft samples and reduce the image resolution. At first the tip is far from the sample surface, bouncing up and down with "free vibration" amplitude. The tip then approaches the

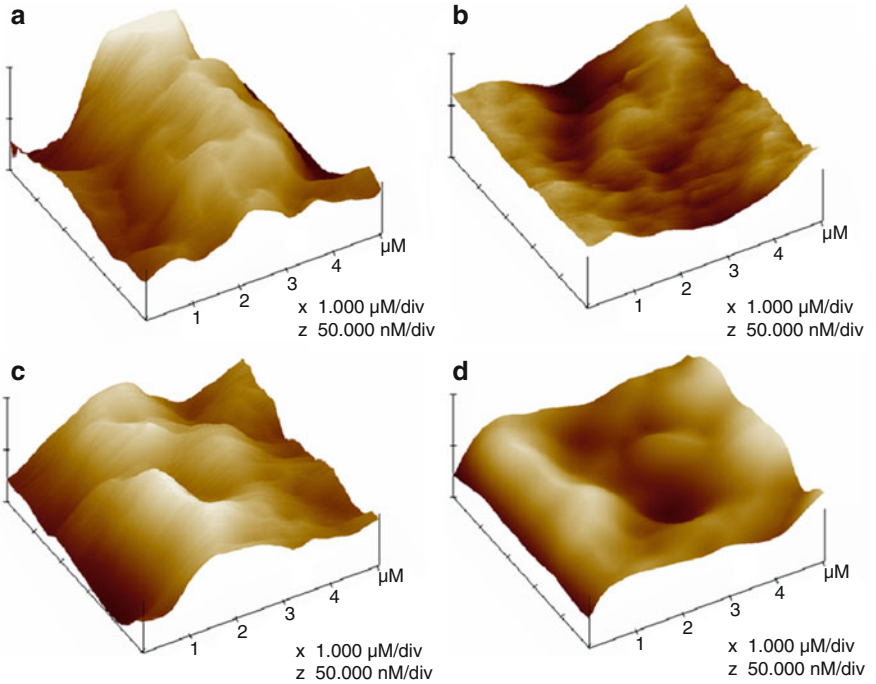

Fig. 15.5 Typical AFM images of uncross-linked (**a** and **b**) and cross-linked (**c** and **d**) isotropic composites with 10% w/w HPC of Avicel fibers: **a** and **c** – bottom surface; **b** and **d** – top surface [12]

sample surface, and because of the tip–surface interaction, the vibration amplitude decreases. During the scanning procedure the vibration amplitude of the tip is kept constant by changing the scanner's height.

Small pieces were cut from each film, glued onto metal discs and attached to a magnetic sample holder located on top of the scanner tube. All the AFM images were taken at 25°C. Typical AFM images are presented in Fig. 15.5. Images of the surfaces of cross-linked and uncross-linked isotropic composite films with 10% (w/w HPC) of fibers are presented, as an example.

Differences in the film-surface morphologies can be expressed in terms of various roughness parameters, such as:

1. The difference between the highest and the lowest points within the given area, z
2. The standard deviation of the z values within the given area (R_q). This parameter is calculated as

$$R_q = \sqrt{\frac{\sum (Z_i - Z_{avg})^2}{N_p}}, \tag{15.1}$$

where Z_i is the current z value, Z_{avg} the average of the z values within the given area and N_p the number of points within the given area.

3. The mean roughness (R_a). This parameter represents the mean value of the surface relative to the center plane, that is, the plane for which the volumes enclosed by the image above and below this plane are equal. It is calculated as

$$R_a = \frac{1}{L_x L_y} \int_0^{L_x} \int_0^{L_y} |f(x,y)| \, dxdy, \tag{15.2}$$

where $f(x, y)$ defines the surface relative to the center plane and L_x and L_y the dimensions of the surface in the x and y directions.

The surface roughness parameters were calculated from the AFM images obtained at several points of each film sample by using an AFM software program.

The roughness parameters depend on the curvature and size of the tip, as well as on the treatment of the captured surface data (plane fitting, flattening, etc.). Therefore, these parameters should not be considered as absolute roughness values. However, in the present study the same tip was used for all films and all captured surfaces were treated in the same way. Tables 15.1 and 15.2 display the roughness parameters calculated from the respective AFM images of both surfaces (top and

Table 15.1 Roughness parameters calculated from the respective AFM images of the uncross-linked isotropic all-cellulosic based composites [12]

Fiber content (% w/w HPC)	Surface	R_a (nm)	z (nm)	R_q (nm)
0	Top	4.70	37.04	5.80
	Bottom	4.99	34.55	7.91
4	Top	3.4	28.76	4.28
	Bottom	14.96	108.1	18.5
10	Top	4.86	43.96	6.24
	Bottom	18.77	167.09	23.59
20	Top	4.50	38.77	5.74
	Bottom	17.19	122.73	20.87
30	Top	9.27	83.86	11.83
	Bottom	22.89	149.99	27.05

Table 15.2 Roughness parameters calculated from the respective AFM images of the cross-linked isotropic all-cellulosic based composites [12]

Fiber content (% w/w HPC)	Surface	R_a (nm)	z (nm)	R_q (nm)
0	Top	1.97	16.52	2.56
	Bottom	2.24	17.95	2.82
4	Top	4.64	48.57	6.06
	Bottom	15.09	119.57	18.59
10	Top	7.85	72.29	10.06
	Bottom	12.04	86.20	15.07
20	Top	9.48	79.48	12.01
	Bottom	18.10	144.81	23.47
30	Top	12.17	132.32	15.63
	Bottom	17.48	199.73	22.96

bottom) of some of the uncross-linked and cross-linked isotropic composites produced.

As seen from Fig. 15.5, all-cellulosic based composites are asymmetric. Bottom surface has a more pronounced roughness, as evidenced by the results presented in Tables 15.1 and 15.2.

The films without fibers have very low values of the parameters R_a and z, revealing relatively uniform structures of the top and bottom surfaces of both uncross-linked and cross-linked films. The very slight differences between the two surfaces can be attributed to the different natures of the air-casting solution and of the Teflon® plate-casting solution interfaces. In contrast to that, the films incorporating fibers display very different values of the roughness parameters for the top and bottom surfaces. In fact, for the uncross-linked composite films the R_a parameter of the bottom surface is nearly four times higher than the corresponding value of the top surface. This is valid up to 20% w/w HPC of fiber incorporation. For 30% w/w HPC of fibers the R_a value of the bottom surface is approximately twice the value of the top surface. These results lead to the conclusion that the fibers are probably preferentially distributed at the bottom of the films.

In the case of the cross-linked composite films, R_a and z parameters of both surfaces of the films seem to increase gradually with the increase of the fiber content, with the bottom surfaces showing always higher values than those of the corresponding top surfaces.

In the cross-linked films, the difference between the roughness parameters of the two surfaces is smaller than that observed in the case of the uncross-linked ones, as shown also in Fig. 15.5. This means that the effect of fiber settling at the bottom surfaces is less pronounced for the cross-linked films, suggesting a better distribution of the fibers over the cross section. This influences the mechanical properties of isotropic all-cellulosic based composites, as discussed later. Also, the asymmetry between top and bottom surfaces will have an impact in gas barrier properties of these composites.

15.4 Mechanical Properties

The mechanical properties (Young's modulus, E, yield stress, σ_y, tensile stress, σ_u, tensile strain, ε_u) of the films were determined using a tensile testing machine from Rheometric Scientific (Minimat-Firmware 3.1). For each composition, three films were obtained and ten samples of 5 × 2 cm were cut from each film and stretched uniaxially at a speed of 5 mm min^{-1} at room temperature. Half of the samples were cut in the shear direction (0°) and the rest perpendicularly to it (90°). Therefore, 30 samples (15 in each direction) of each composition were tested in order to take into account the inherent variability of these systems. All the parameters were calculated for a 95% confidence interval for the mean.

Mechanical parameters of isotropic all-cellulosic based composites are invariant regardless of the direction of measurement (0° or 90°). It has been shown [12] that

the inclusion of fibers in a HPC matrix produces composites with superior mechanical properties, which can be improved by cross-linking. Mechanical data seem to indicate that the elastic deformation of the isotropic cross-linked composites is predominantly dominated by the fiber content, while the cross-linking affects mainly the plastic deformation.

Mechanical properties of anisotropic all-cellulosic based composites are presented in Table 15.3.

In all cases the composite films were found to be more resistant in the shear direction and consequently less deformable. The high anisotropy of the mechanical properties is evident from the results of Table 15.3, where it can be seen that Young's modulus, yield stress and ultimate tensile strength are higher in the shear direction.

For comparison, Table 15.4 presents the mechanical properties of anisotropic and uncross-linked isotropic all-cellulosic based composites.

Table 15.4 clearly shows that anisotropic composite films present better mechanical properties. It is worth noting that anisotropic composites also have higher Young's modulus, yield stress and ultimate tensile strength than cross-linked isotropic homologues [13]. This, along with results presented in Table 15.4, seems to indicate that the mechanical properties of these all-cellulosic based composites depend on matrix anisotropy and fiber orientation rather than on cross-linking.

In fact, due to the same chemical nature of fibers and matrix, an efficient matrix-fiber stress transfer will probably be ensured by hydrogen bonds between the two components.

Table 15.3 Mechanical properties of anisotropic all-cellulosic based composite films, measured in the shear direction (0°) and perpendicular to it (90°)

Fiber content (% w/w HPC)	E (MPa)		σ_y (MPa)		σ_u (MPa)		ε_u (%)	
	0°	90°	0°	90°	0°	90°	0°	90°
0	274	130	7.7	4.1	12.8	5.1	28.0	54.0
2	350	150	9.3	6.2	14.0	7.9	14.0	40.4
4	431	160	9.9	6.6	18.0	7.5	16.0	35.6
6	470	214	12.7	6.2	28.7	9.1	15.5	20.0
10	481	240	12.0	7.8	19.7	10.4	17.0	16.6
12	441	193	12.4	7.9	19.1	10.0	18.0	15.5

Presented results are average values with an error of about 10% [14]

Table 15.4 Comparison of the mechanical properties of uncross-linked isotropic (I) and anisotropic (A) all-cellulosic based composite films

Fiber content (% w/w HPC)	E (MPa)		σ_y (MPa)		σ_u (MPa)	
	I	A	I	A	I	A
0	109	274	3.5	7.7	5.2	12.8
2	145	350	4.8	9.3	5.9	14.0
4	155	431	5.3	9.9	6.4	18.0
6	–	470	–	12.7	–	28.7
10	213	481	6.1	12.0	8.1	19.7
12	–	441	–	12.4	–	19.1

Presented results are average values obtained in the shear direction with an error of about 10% [14]

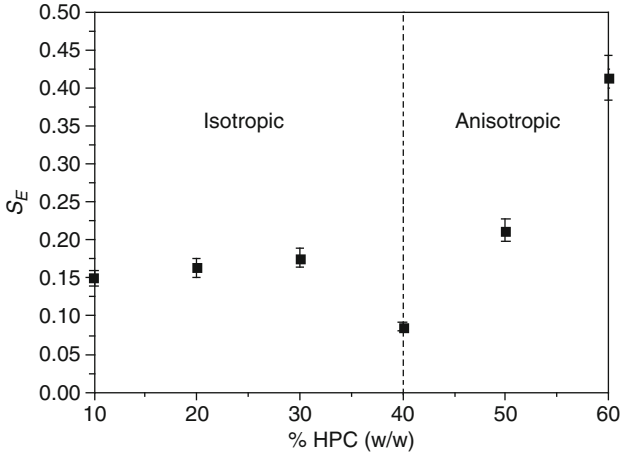

Fig. 15.6 Plot of the order parameter, *S*, of all-cellulosic based composites (2% w/w HPC of Avicel fibers), as a function of HPC content. Isotropic and anisotropic composites are marked [13]

From the mechanical properties of all-cellulosic based composites, an order parameter, S_E, was calculated using (15.3) [20]:

$$S_E = \frac{((E_{0^\circ}/E_{90^\circ}) - 1)}{((E_{0^\circ}/E_{90^\circ}) + 2)} \tag{15.3}$$

The variation of S_E with HPC concentration in the precursor solutions for composites preparation is shown in Fig. 15.6. Results presented refer to composites with 2% w/w HPC of Avicel fibers, but similar trends are observed for the other fiber contents.

This order parameter is a macroscopic measure of the anisotropy of the composites but it, nevertheless, reflects the microstrutural organization of the all-cellulosic based composites. The variation of S_E with HPC content is similar to that observed for *S* (Fig. 15.3) and Δn (Fig. 15.4). Table 15.3 (and also Fig. 15.2c) shows that HPC matrix (0% w/w HPC of fibers) is clearly anisotropic and therefore the anisotropy in these composites arises from the synergy between the liquid crystalline character of the matrix and the fiber orientation.

15.4.1 Modeling of Mechanical Properties

In this section the mechanical properties (Young's modulus) and the strength of the fiber–matrix interface (quality of the interface) of isotropic all-cellulosic based composites will be analyzed using theoretical models existing in literature. For the anisotropic composites such an approach was not performed. The anisotropy in these composites arises mainly from the liquid crystalline character of the matrix,

which in turn induces fiber orientation. Liquid crystalline materials have complex structure and dynamics and there are no available theoretical models for composites with this kind of matrices.

Two theoretical models were used to predict Young's modulus of isotropic all-cellulosic based composites:

1. Cox "shear-lag" model [21] that takes into account the geometrical arrangement of the fibers.
2. Modified Halpin–Tsai equations [22, 23], which are dependent on fiber packing efficiency.

When SFCs are stressed, the stresses are transferred to the fibers by shear at the fibers surface, which causes fiber deformation. To estimate the Young's modulus of SFCs, Cox [21] proposed a model that assumes a completely elastic transfer of stresses from the matrix to the fiber. By averaging the stress distribution within the fibers, the theory predicts the Young's modulus for aligned SFCs, in the direction of alignment, to be equal to:

$$E = \chi_2 \upsilon_f E_f + (1 - \upsilon_f) E_m, \tag{15.4}$$

where v_f refers to the volume fraction of fibers; E_f and E_m to the Young's modulus of fibers and matrix, respectively. The parameter χ_2 is a fiber-length correction factor that depends on fiber aspect ratio, fiber packing (center-to-center distance), matrix shear modulus and fibers' Young modulus. When the fiber length is not uniform (as in the case of isotropic all-cellulosic based composites) χ_2 can be obtained as a weighted sum, with the weights determined by the fiber-length distribution [24].

When fibers are not perfectly aligned with the direction of the modulus estimate, an orientation-efficiency factor, χ_1, is added to (15.4) [25] and Young's modulus will be then deduced from (15.5).

$$E = \chi_1 \chi_2 \upsilon_f \mathrm{E_f} + (1 - \upsilon_f) E_m, \quad 0 < \chi_1 < 1 \tag{15.5}$$

The orientation-efficiency factor was theoretically determined by Krenchel [26]. For in-plane uniformly distributed fiber orientations, the factor is 3/8 and for 3D uniform fiber orientation distribution is 1/5. In practice, the determination of fiber orientation distribution is normally done by image analysis of different sections of the composites [27]. In the case of all-cellulosic based composites this would be impossible, due to their thickness. In this case, the value of the orientation-efficiency factor was taken as the value of the order parameter, S, determined by SALS.

The most used materials property model, particularly in engineering design applications, is the Halpin–Tsai model [28] or Halpin–Tsai equations as they are often termed. Although the model has limitations with respect to its rigor and accuracy, its main advantage is the simple universal form of expressions in its formulation, and its applicability to a number of different material forms and their *moduli*. The general form of Halpin–Tsai equations is given by:

$$\frac{M}{M_{\mathrm{m}}} = \frac{1 + AB\upsilon_{\mathrm{f}}}{1 - B\upsilon_{\mathrm{f}}} \quad \wedge \quad B = \frac{(M_{\mathrm{f}}/M_{\mathrm{m}}) - 1}{(M_{\mathrm{f}}/M_{\mathrm{m}}) + A}, \tag{15.6}$$

where M is the composite modulus (plane strain bulk modulus, longitudinal and transverse shear modulus or longitudinal and transverse Young modulus), M_{f} the corresponding fiber modulus and M_{m} the corresponding matrix modulus. A is a measure of the reinforcement geometry and loading and for longitudinal Young's Modulus and it will take the value of $2l/d$ (l/d is the fiber aspect ratio, which for Avicel fibers as the value of 5). Halpin–Tsai equations have been found to be inaccurate at higher volume fraction of fibers, because it does not take into account the limit in maximum packing fraction in a real system. The problem was addressed by Nielsen [22] who produced the amended form of the generalized equation, presented in expression (15.7).

$$\frac{M}{M_{\mathrm{m}}} = \frac{1 + AB\upsilon_{\mathrm{f}}}{1 - B\psi\upsilon_{\mathrm{f}}} \quad \wedge \quad \psi = \frac{1 - \varphi_{\mathrm{m}}}{\varphi_{\mathrm{m}}^2}\upsilon_{\mathrm{f}} \tag{15.7}$$

The introduction of the parameter ψ takes into account the maximum packing fraction ϕ_{m}. For cubic packing $\phi_{\mathrm{m}} = 0.785$, whilst for hexagonal packing$\phi_{\mathrm{m}} = 0.907$ [23]. For SFCs, where fibers are generally more random in their arrangement, ϕ_{m} can take significantly lower values. Because of the uncertainty of the maximum packing fraction and its dependence on both alignment and aspect ratio, ϕ_{m} is used as an empirical fitting factor in the materials modeling process.

The results of Young's modulus prediction, according to (15.5) and (15.7), for uncross-linked isotropic all-cellulosic based composites are presented in Figs. 15.7 and 15.8. The modeling parameters used for (15.5) are listed in Table 15.5.

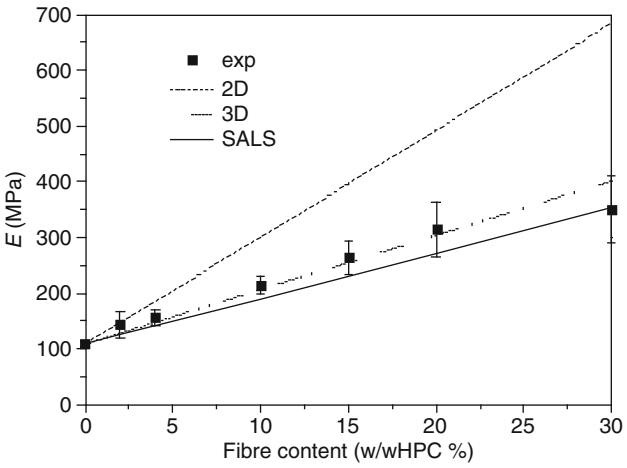

Fig. 15.7 Variation of the Young's modulus of uncross-linked isotropic all-cellulosic based composites with fiber content. Experimental values (exp) are compared to those obtained from (15.5) using different values of χ_1 as explained in Table 15.5

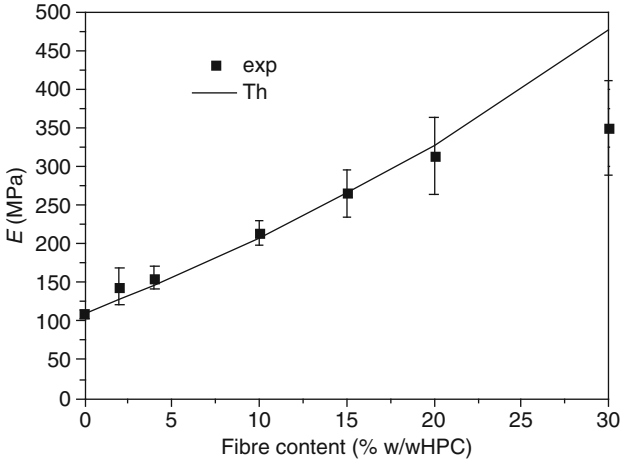

Fig. 15.8 Variation of the Young's modulus of uncross-linked isotropic all-cellulosic based composites with fiber content. Experimental values (exp) are compared to theoretical predictions (Th) obtained from (15.7). Note that fiber content is presented in wt% but all calculations were made using the volume fraction of fibers [13]

Table 15.5 Fitting parameters used in (15.5) [13]

Fitting parameters	Observations
$E_f = 25$ GPa	Value of E_f from [29]
$E_m = 109$ MPa	Values of the orientation efficiency factor, χ_1, are given for (a) in-plane fiber orientation (2D) [26], (b) 3D uniform fiber orientation (3D) and (c) fiber orientation parameter determined by light scattering (SALS)
$\chi_2 = 0.23$	
$\chi_1 = \begin{cases} 0.375 & (2D) \\ 0.20 & (3D) \\ 0.17 & (SALS) \end{cases}$	

Figure 15.7 displays the dependence between the Young's modulus of uncross-linked isotropic composites and their fiber content and shows that an in-plane distribution of the fibers in the composites is highly improbable. The same conclusion was drawn from the fit of the experimental data of the cross-linked composites. The predicted values of the Young's modulus for a 3D uniform distribution of the fibers are closer to that of the average values determined experimentally. Avicel fibers are not perfect rod objects (low aspect ratio: $l/d \sim 5$), being this the probable justification for a preferred 3D arrangement.

Results obtained using the order parameter determined by SALS, as the value of the orientation efficiency factor, are always closer to the lower bound values of the Young's modulus of the composites. The order parameter is determined as a function of the angle of the fibers to the shear direction, meaning that its value will be more accurate for an in-plane distribution of the fibers. This would probably be the case if the fibers had higher aspect ratio. Nevertheless, SALS seems to be a promising

technique in order to determine the orientation efficiency parameter for composite systems like these, i.e., thin composite materials.

The fit of the Young's modulus experimental values using (15.7) allowed the determination of the maximum packing fraction of fibers, ϕ_m. The results of this fit for the uncross-linked composites are presented, as an example, in Fig. 15.8. From the fits, values of 0.81 and 0.51 for ϕ_m were obtained for uncross-linked and cross-linked isotropic all-cellulosic based composites, respectively.

High values of ϕ_m for the uncross-linked composites may be related to the preferred 3D packing of the fibers. Lower value of the maximum packing fraction in cross-linked composites confirms the more uniform distribution of the fibers over its cross section, as deduced from AFM measurements. The more efficient packing of the fibers in cross-linked composites is most probably the main reason for the better mechanical performance of these materials.

The second reason for the better mechanical properties of cross-linked composites is the higher quality of the fiber–matrix interface which improves the stress transfer efficiency between these two components.

The strength of the interaction was quantitatively characterized for isotropic uncross-linked and cross-linked all-cellulosic based composites with the help of a semi-empirical model taken from literature [30, 31].

The model describes the composition dependence of tensile yield stress or tensile strength of particulate filled polymers. The expression for yield stress takes the form:

$$\sigma_y = \sigma_{y0} \frac{1 - \upsilon_f}{1 + 2.5\upsilon_f} \exp(B\upsilon_f), \tag{15.8}$$

where σ_y and σ_{y0} are the yield stresses of the composite and that of the polymer matrix, respectively, v_f is the volume fraction of the filler in the composite and B the parameter characterizing fiber–matrix interaction.

The term $(1 - \upsilon_f)/(1 + 2.5\upsilon_f)$ takes into account the decrease of the effective load-bearing cross-section owing to the introduction of the filler into the polymer matrix.

Equation (15.8) can be rearranged to take the linear form

$$\ln\left(\frac{\sigma_y}{(1 - \upsilon_f)/1 + 2.5\upsilon_f}\right) = \ln(\sigma_{y0}) + B\upsilon_f, \tag{15.9}$$

where the term $\sigma_y/((1 - \upsilon_f)/(1 + 2.5\upsilon_f))$ is a reduced yield stress.

A semi-log plot of the reduced yield stress versus fiber content for uncross-linked and cross-linked composites is presented in Fig. 15.9. A maximum of15% (w/w HPC) of fibers was considered since, as seen from Fig. 15.8, an efficient packing (in terms of mechanical performance of the composites) is attained up to 15–20% (w/w HPC) of fibers.

The values of B and σ_{y0}, obtained from the fit of the experimental data with (15.9) are presented in Table 15.6.

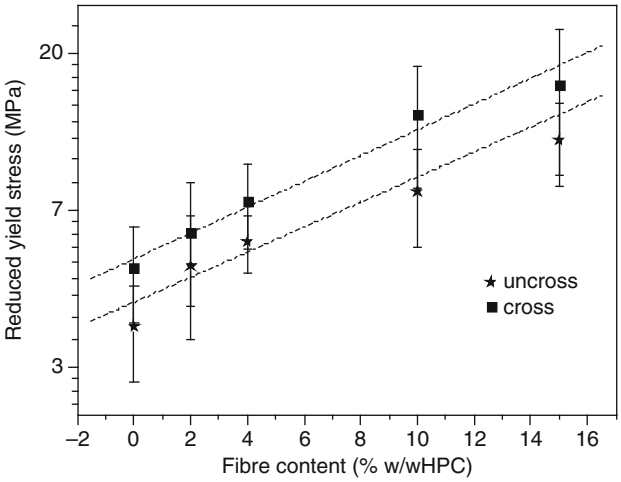

Fig. 15.9 Semi-log plot of the reduced yield stress versus fiber content for uncross-linked (uncross) and cross-linked (cross) isotropic all-cellulosic based composites. *Dash lines* represent the linear fit, according to (15.9). Note that fiber content is presented in wt% but all calculations were made using the volume fraction of fibers

Table 15.6 Values of B and σ_{y0} for isotropic all-cellulosic based composites obtained from the linear fits of (15.9)

	B	σ_{y0} (MPa)	R^2
Uncross-linked	1.66 ± 0.04	3.80 ± 0.31	0.985
Cross-linked	2.16 ± 0.06	4.95 ± 0.40	0.991

The corresponding correlation coefficients (R^2) are presented

Values obtained for the matrix yield stress, σ_{y0}, are very close to those obtained experimentally (uncross = 3.51 ± 0.4 MPa; cross = 5.10 ± 0.6 MPa), which confirms the validity of the model to these composites. Higher B values for cross-linked isotropic all-cellulosic based composites show that the interface is stronger in these materials, which is a consequence of the possibility of establishing covalent linkages between fibers and matrix.

15.5 Gas Barrier Properties

Gas barrier properties were evaluated to access the potential of isotropic all-cellulosic based composites for packaging applications. The mechanical properties, flexibility and biocompatibility of these materials can be useful, in particular, for food packaging. Due to the nature of the envisaged application insoluble materials are required. This requisite is only fulfilled by cross-linked composites and, therefore, we have decided to subject only cross-linked films for gas permeation measurements.

Gas permeation experiments were carried out for carbon dioxide, oxygen and nitrogen. The method used to measure the gas permeability was the constant pressure or variable volume method. For the measurements a home-made system was used [32]. It comprised a two-compartment flat sheet permeability cell .The feed stream circulates in the bottom compartment tangentially to the composite films and permeates through them to be collected in the top compartment where a flowmeter is connected. Due to the asymmetry of the composites the permeation experiments were carried out both for the top and bottom surfaces of the composite films facing the feed stream.

The feed pressure used ranged from 1 to 4 bar and the effective membrane surface area was 9.07 cm^2. The gas permeability was determined by the following equation:

$$P = \frac{qL}{(P_1 - P_2)At}, \tag{15.10}$$

where P is the gas permeability (cm^3 (STP) cm cm^{-2} s^{-1} cm Hg^{-1}), q/t the volumetric flow rate of the gas permeation, L the membrane thickness, P_1 and P_2 the pressures and A the effective membrane area.

As an example, the permeability to carbon dioxide of the isotropic HPC matrix is shown in Fig. 15.10, as a function of feed pressure. It was observed that the permeabilities decrease in the order of $P(CO_2) > P(O_2) > P(N_2)$. The higher CO_2 permeability is probably due to the relative high solubility of this gas in the HPC matrix when compared with O_2 and N_2. The permeability of CO_2, O_2 and N_2 increases linearly with the upstream pressure and it is always higher for the bottom surface. The data collected in Table 15.2 show that HPC matrix (0% w/w HPC) has

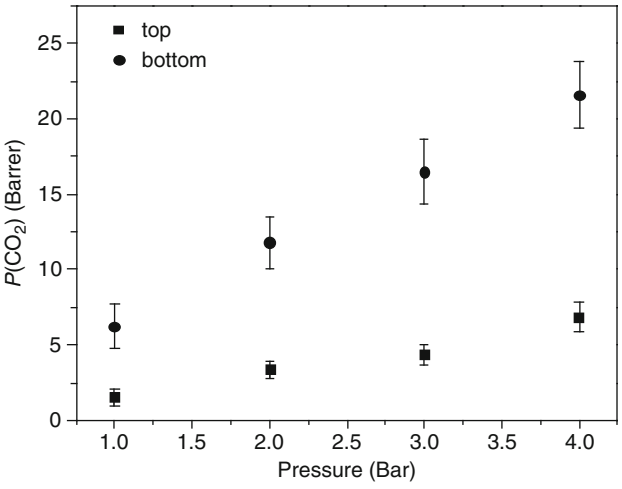

Fig. 15.10 Carbon dioxide permeability of the isotropic HPC matrix versus feed pressure [13]

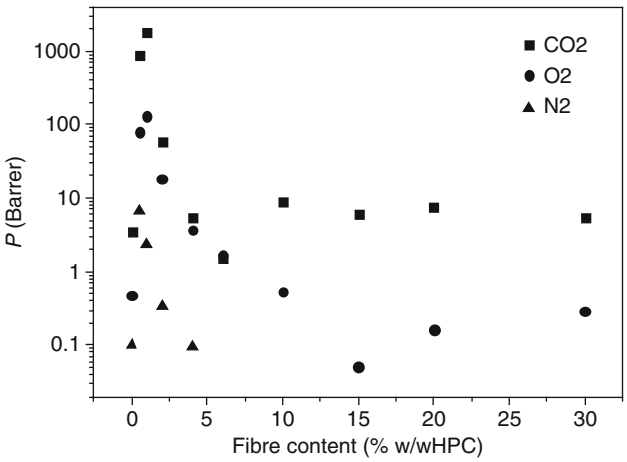

Fig. 15.11 Variation of gas permeability (CO_2, O_2 and N_2) of the cross-linked isotropic all-cellulosic based composites with fiber content [13]

relatively uniform structures of the top and bottom surfaces. However, roughness parameters are slightly higher for the bottom side, and this is probably the cause for the observed surface higher permeability to the three gases.

The permeability of the composites towards the three gases is higher than that of the matrix, as shown in Fig. 15.11. The introduction of 0.5–1% (w/w HPC) of fibers promotes a two to three orders of magnitude increase in top surface permeability to the three gases. For the bottom surface a similar trend was observed and, as for the HPC matrix, higher values of the permeabilities were obtained. The explanation of such behavior lies probably in the molecular structure of these materials. In polymeric systems, the gas permeability is related to the mobility of the macromolecules [33]. Therefore, lower permeability values of the HPC matrix should be related to the low mobility of the polymeric chains, induced by cross-linking. As referred before, the diisocyanates promote cross-linking of the matrix and fiber–matrix covalent bonds. In the presence of fibers part of the diisocyanate in the system will be consumed in fiber–matrix coupling, which will locally increase the mobility of the HPC macromolecules.

The density of the cross-links and the fiber–matrix covalent links are dictated by the amount of diisocyanate used. It's also important to notice that –OH groups of HPC are more accessible, therefore most of the diisocyanate is consumed in cross-linking of HPC. The maximum permeability obtained for 0.5–1% (w/w HPC) of fibers is probably related to the maximum density of fiber–matrix covalent links allowed in the system, which is likely dependent on the amount of diisocyanate used. The increase of the fiber content leads firstly to the settling of fibers at the bottom surface and then to its distribution over the volume of the composites. Such fiber packing mode may be responsible for the decrease in the diffusivity of the gases, which in turn causes the decrease in permeability.

Table 15.7 Oxygen permeability of selected polymers used in food packaging [34]

	PET	LDPE	HDPE	PP	PS
$P(O_2)$/Barrer	0.01–0.013	0.85–1.18	0.34–0.68	0.51–0.85	0.85–1.35

PET poly(ethylene terephthalate), *LDPE* low-density polyethylene, *HDPE* high-density polyethylene, *PP* polypropylene, *PS* polystyrene

Table 15.8 Oxygen permeability of cross-linked isotropic all-cellulosic based composites

Fiber content (% w/w HPC)	0	0.5	1	2	4	6	10	15	20	30
$P(O_2)$/Barrer	0.48	78.1	131	18.2	3.64	1.66	0.54	0.05	0.16	0.29

The permeability of the packaging material is one of the most critical features of the package. In particular, oxygen can promote oxidation reactions, altering the quality of the food and its shelf life. Any candidate for food packaging material should therefore be an oxygen high barrier. In Tables 15.7 and 15.8 oxygen permeability for selected polymers [34] used in food packaging and for cross-linked isotropic all-cellulosic based composites, respectively, are presented.

The cross-linked HPC matrix and composites with 10–30% of fibers have similar or even lower oxygen permeabilities than those of most common polymers used in food packaging (LDPE, HDPE, PP and PS), which makes these materials good candidates for that application.

15.6 Further Developments

All-cellulosic based composite films can be prepared from either isotropic or anisotropic cellulosic derivatives solutions. However, these composites cannot compete with mechanical properties of cellulose nanofiber reinforced composites. Pioneering studies reported by Favier et al. [35, 36], showed that small amounts of cellulose tunicate whiskers resulted in dramatic improvements in modulus above the glass transition temperature of an amorphous polymer matrix, due to the percolation of the cellulose nanofibers. Also recently, a completely new route to cellulose-based composites was proposed by Nishino and Arimoto [37], Soykeabkaew et al. [38–40]. They focused on approaches following self-reinforcing polymer concepts [41, 42] to create composites that often outperform traditional nanofiber reinforced composites [38, 40].

The use of cellulosic nanofibers in the production of all-cellulosic based composites can greatly improve the mechanical performance of these composites. With these nanofibers and a cellulosic anisotropic matrix a synergy between the percolation of the nanofibers and its matrix-induced orientation can lead to composites with enhanced mechanical properties.

A better mechanical performance of the all-cellulosic composites reported here could also be achieved taking advantage of liquid crystalline properties of aqueous suspensions of acid hydrolysed microcrystalline cellulose (MCC) [43, 44]. A chiral ordering of MCC aqueous suspensions was observed for various cellulose origins

such as wood, cotton, ramie, and bacterial cellulose. The authors also reported the conservation of this structure after water evaporation. Orts et al. [45] also verified that these cellulose microfibrils can be oriented by shear. This may lead to the future development of high-performance composites, fully anisotropic and highly ordered, based on liquid crystalline phases of both cellulosic derivative and cellulose fibers.

15.7 Conclusion

All-cellulosic based composites exhibit very interesting mechanical and gas barrier properties along with biocompatibility, making them promising candidates for applications in food packaging. The mechanical properties can be tuned in function of the anisotropy of the matrix. Future developments towards high-strength materials can be envisaged by taking full advantage of the orientacional liquid crystalline properties of both the matrix and the fibers.

Acknowledgments This work was partially sponsored by Portuguese Science and Technology Foundation through project PTDC/CTM/099595/2008.

References

1. Manson JA, Sperling LH (1976) Polymer blends and composites. Plenum, New York
2. Eichhorn SJ, Dufresne A et al (2010) Review: current international research into cellulose nanofibers and nanocomposites. J Mater Sci 45:1–33
3. Berglund LA, Peijs T (2010) Cellulose biocomposites-from bulk moldings to nanostuctured systems. MRS Bull 35:201–207
4. Ly B, Thielemans W et al (2008) Surface functionalization of cellulose fibers and their incorporation in renewable polymeric matrices. Compos Sci Technol 68:3193–3201
5. Peijs T, Baillie C (eds) (2003) Eco-composites. Compos Sci Technol 63:1223–1336
6. Mohanty AK, Misra M et al (2000) Biofibers, biodegradable polymers and biocomposites. An overview. Macromol Mater Eng 276(277):1–24
7. Gassan J, Bledzki AK (1999) Composites reinforced with cellulose based fibers. Prog Polym Sci 24:221–274
8. Lu JZ, Wu Q et al (2000) Chemical coupling in wood fiber and polymer composites: a review of coupling agents and treatments. Wood Fiber Sci 32:88–108
9. Belgacem MN, Gandini A (2005) The surface modification of cellulose fibers for use as reinforcing elements in composite materials. Compos Interf 12:41–75
10. Borges JP, Godinho MH et al (2001) New bio-composites based on short fiber reinforced hydroxypropylcellulose films. Compos Interf 8:233–241
11. Borges JP, Godinho MH et al (2001) Cellulose-based composite films. Mech Compos Mater 37:257–264
12. Borges JP, Godinho MH et al (2004) Tensile properties of cellulose fiber reinforced hydroxypropylcellulose films. Polym Compos 25:102–110
13. Borges JP (2004) PhD Thesis, FCT-UNL
14. Borges JP, Godinho MH (2008) Cellulose-based anisotropic composites. Mater Sci Forum 587–588:604–607

15. Aharoni SM, Walsh EK (1979) Rigid backbone polymers. 4. Solution properties of two lyotropic mesomorphic poly(isocyanates). Macromolecules 12:271–276
16. Ernst B, Navard P (1989) Band textures in mesomorphic (hydroxypropyl) cellulose solutions. Macromolecules 22:1419–1422
17. Viney C, Putnam W (1995) The banded microstructure of sheared liquid-crystalline polymers. Polymer 36:1731–1741
18. Riti JB, Cidade MT et al (1997) Shear induced textures of thermotropic acetoxypropylcellulose. J Rheol 41:1247–1259
19. Godinho MH, Fonseca JG et al (2002) Atomic force microscopy study of hydroxypropylcellulose films prepared from liquid crystalline aqueous solutions. Macromolecules 35:5932–5936
20. Schätzle J, Finkelmann H (1987) State of order in liquid crystalline elastomers. Mol Cryst Liq Cryst 142:85–100
21. Cox HL (1952) The elasticity and strength of paper and other fibrous materials. Br J Appl Phys 3:72–79
22. Nielsen LE (1970) Generalized equation for the elastic moduli of composite materials. J Appl Phys 41:4626–4627
23. Nielsen LE, Landel RF (1994) Mechanical properties of polymers and composites. Dekker, New York
24. Piggott MR, Ko M et al (1993) Aligned short-fiber reinforced thermosets: experiments and analysis lend little support for established theory. Compos Sci Technol 48:291–299
25. Hull D (1981) An introduction to composite materials. Cambridge University Press, London
26. Krenchel H (1964) Fiber reinforcement. Akademisk Forlag, Copenhagen
27. De SK, White JR (eds) (1996) Short fiber-polymer composites. Woodhead, Cambridge, England
28. Halpin JC, Kardos JL (1976) The Halpin-Tsai equations: a review. Polym Eng Sci 16:344–352
29. Eichhorn SJ, Young RJ (2001) The Young's modulus of a microcrystalline cellulose. Cellulose 8:197–207
30. Turcsányi B, Pukánszky B et al (1988) Composition dependence of tensile yield stress in filled polymers. J Mater Sci Lett 7:160–162
31. Pukánszky B (1990) Influence of the interface interaction on the ultimate tensile properties of polymer composites. Composites 21:255–262
32. Queiroz DP, de Pinho MN (2005) Structural characteristics and gas permeation properties of polydimethylsiloxane/poly(propylene oxide) urethane/urea bi-soft segment membranes. Polymer 46:2346–2353
33. Mulder M (1996) Basic principles of membrane technology. Kluwer, London
34. Delassus P (1997) Barrier properties. In: Brody A, Marsh K (eds) The Wiley encyclopedia of packaging technology, 2nd edn. New York, Wiley
35. Favier V, Canova GR et al (1995) Nanocomposite materials from latex and cellulose whiskers. Polym Adv Technol 6:351–355
36. Favier V, Chanzy H et al (1995) Polymer nanocomposites reinforced by cellulose whiskers. Macromolecules 28:6365–6367
37. Nishino T, Arimoto N (2007) All-cellulose composite prepared by selective dissolving of fiber surface. Biomacromolecules 8:2712–2716
38. Soykeabkaew N, Arimoto N et al (2008) All-cellulose composites by selective dissolution of aligned lingo-cellulosic fibers. Compos Sci Technol 68:2201–2207
39. Soykeabkaew N, Sian N et al (2009) All-cellulose nanocomposites by surface selective dissolution of bacterial cellulose. Cellulose 16:435–444
40. Qin C, Soykeabkaew N et al (2008) The effect of fiber volume fraction on the properties of all-cellulose composites. Carbohydr Polym 71:458–467
41. Alcock B, Cabrera NO et al (2006) Low velocity impact performance of recyclable all-polypropylene composites. Compos Sci Technol 66:1724–1737

42. Alcock B, Cabrera NO et al (2007) The effect of temperature and strain rate on the mechanical properties of highly oriented polypropylene tapes and all-polypropylene composites. Compos Sci Technol 67:2061–2070
43. Revol JF, Bradford H et al (1992) Helicoidal self-ordering of cellulose microfibrils in aqueous suspension. Int J Biol Macromol 14:170–172
44. Habibi Y, Lucia LA et al (2010) Cellulose nanocrystals: chemistry, self-assembly and applications. Chem Rev. doi:10.1021/cr900339w
45. Orts WJ, Godbout L et al (1998) Enhanced ordering of liquid crystalline suspensions of cellulose microfibrils: a small angle neutron scattering study. Macromolecules 31:5717–5725